

Pressure drop-based determination of dynamic interfacial tension of droplet generation process in T-junction microchannel

Xueying Wang · Antoine Riaud ·
Kai Wang · Guangsheng Luo

Received: 11 December 2013 / Accepted: 20 June 2014 / Published online: 28 June 2014
© Springer-Verlag Berlin Heidelberg 2014

Abstract The dynamic interfacial tension caused by the lower surfactant adsorption rate than the droplet generation rate is an important issue in microfluidic study. A pressure drop measurement method is proposed to determine the dynamic interfacial tension during the droplet generation process at a T-junction microchannel. Experimental results show that in the transitional flow regime between squeezing and dripping, the maximum pressure drop appears at the end of filling stage defined by Glawdel et al. (Phys Rev E 85(1):016322, doi:10.1103/PhysRevE.85.016322, 2012a), as the liquid–liquid interface starts to leave the side channel. This pressure drop is composed of Laplace pressure and flow resistance. Using the pressure drop measurements, the contribution of fluctuated Laplace pressure is confirmed, and the instantaneous interfacial tension at the maximum pressure drop is calculated. Although the final droplet volume shows that almost no interfacial tension difference exists at the breakup moment, the pressure drop result unveils some discrepancies. Experimental results reflect the variation of dynamic interfacial tension is a quasi-surfactant diffusion-controlled process when the main channel is totally blocked by the growing droplet at the end of filling stage. However, this quasi-diffusion model no longer works as the droplet does not block the channel, due to the strong convection of two-phase flow. Surfactant sodium dodecyl sulfate and Tween 20 also show different micelle dissociation rates in the variation test of concentrations.

Keywords Dynamic interfacial tension · Pressure drop · Surfactant · T-junction microchannel · Squeezing to dripping transition

1 Introduction

In recent years, microfluidics has emerged as a new research field and has enjoyed prosperous development ever since 1990s (Kobayashi et al. 2001; Cristini and Tan 2004; Thorsen et al. 2001; Xu and Nakajima 2004). It has applicable potential in various fields, such as chemistry, material, biological analysis as well as information technology (Whitesides 2006; Thorsen et al. 2002; Beebe et al. 2002; Wainright et al. 2003). Fundamental research of microflow offers potential applications with a solid theoretical basis and points out possible directions. T-junction microchannel is a widely used microfluidic structure for the generation of mono-dispersed droplets or bubbles thanks to its simple structure and relatively well-studied flow rules (Christopher and Anna 2007; Xu et al. 2008). Capillary number, which represents the ratio of shearing force to interfacial tension ($Ca = \mu u / \gamma$), is the most important parameter in the study of microfluidics. Studies show that in a T-junction microchannel, the droplet size is mainly influenced by the flow rate ratio of dispersed phase to continuous phase when capillary number is small ($Ca < 0.01$) (Garstecki et al. 2006), while in case of bigger value of capillary number ($Ca > 0.1$), the competition between the shearing effect from the continuous phase and the interfacial tension becomes the mainly influential factor (Christopher et al. 2008).

In most microfluidic processes, surfactants play an important role in reducing interfacial tension between two immiscible phases, facilitating the droplet deformation and breakup and stabilizing the emulsion (Baret 2012). In a

X. Wang · A. Riaud · K. Wang (✉) · G. Luo (✉)
The State Key Laboratory of Chemical Engineering,
Department of Chemical Engineering, Tsinghua University,
Beijing 100084, China
e-mail: kaiwang@tsinghua.edu.cn

G. Luo
e-mail: gsluo@tsinghua.edu.cn

T-junction microchannel, different from traditional batch process, the generation of droplets is continuous. This leads to a phenomenon called dynamic interfacial tension, which is a result of the longer surfactant adsorption time compared to the short droplet formation time. This phenomenon has been reported by Baret et al. (2009), where he studied the droplet formation process and stabilization process separately, demonstrating the dynamics of surfactant adsorption plays a significant role in the droplet stabilization. Another study carried out by van der Graaf et al. (2004) confirmed the influence of dynamic interfacial tension on droplet formation in membrane emulsification process, which has a similar generation mechanism as the droplet generation in T-junction microchannel. Different ways of measurement have been taken to figure out this value in microfluidic studies, including the works of Wang et al. (2009) and Dong et al. (2013) trying to determine the interfacial tension at the rupturing moment from droplet size in T-junction and co-flowing dripping flows; the work of Glawdel and Ren (2012) determining the interfacial tension in droplet growing process from image analysis and theoretical models in the transition flow of squeezing and dripping; and the work of Brosseau et al. (2014) determining the interfacial tension on generated droplet from its deformability in microchannel.

Previous works on the dynamic interfacial tension are almost based on droplet diameter measurement or relative complete image analysis from microscope experiments. In this study, we introduce a pressure drop measurement method assisted by simple image analysis, which could be a good tool to determine the dynamic interfacial tension during the droplet generation process. According to the analysis of Riaud et al. (2013) based on the model of van Steijn et al. (2010), the pressure drop between T-junction microchannel (ΔP) equals to the Laplace pressure in the growing droplet, which is a function of interfacial tension and interface curvature radii during the droplet generation process as shown by Eq. 1,

$$\Delta P = \gamma \cdot (1/R_A + 1/r_A - 1/R - 1/r) \quad (1)$$

where R_A and r_A are the interface curvature radii of droplet head on width and depth directions, and R and r are the interface curvature radii of droplet tail on the same two directions. The interfacial tension at any time during the droplet generation process can be calculated in theory from the interface curvature and accurate enough pressure drop measurements. In the recent years, studies have been effectuated to plot out the pressure drop waveform of different flow patterns in T-junction microchannel by simulation and experiments (Abate et al. 2012; Xu et al. 2014). In our research group, a meaningful method in measuring pressure drop is given by the previous work of Riaud et al. (2013), where they detected the pressure drop on several Pascal with

an accuracy of 1 Pa. We aim to use this measuring method to study the dynamic interfacial tension during the droplet generation process with synchronized videos in this study.

2 Experimental section

2.1 Materials

The systems we used were liquid–liquid two-phase systems comprised of n-octane (Sinopharm Chemical Reagent Co., Ltd., China) as the dispersed phase and a serous of surfactant aqueous solutions as the continuous phase. We chose two surfactants to effectuate experiments separately. One is sodium dodecyl sulfate (SDS, CMC = 9.7 mmol/L, about 0.28 wt% in water, Mikati 1993), which has a relatively high monomer diffusion coefficient ($8.0\text{--}11.2 \times 10^{-10} \text{ m}^2/\text{s}$, Glawdel and Ren 2012) due to its small molecular weight (288.4 g/mol), and the other is Tween 20 (CMC = 0.058 mmol/L, about 0.07 wt% in water, Carnero Ruiz et al. 2003), owing a relatively low monomer diffusion coefficient ($9.3 \times 10^{-11} \text{ m}^2/\text{s}$, Carnero Ruiz et al. 2003) and bigger molecular weight (1,227.2 g/mol). All surfactant solutions were premixed thoroughly using a magnetic stir plate until transparent. Some of their physical properties are provided in Table 1, where the viscosities were measured with an electromagnetically spinning sphere viscometer (Brookfield LVDV-II+PRO, USA), and the static interfacial tensions as well as the contact angles of octane on microchannel wall with various surfactant solutions were measured with a sessile tensiometer (OCAH200, DataPhysics Instruments GmbH, Germany). In this study, all the surfactant concentrations were much higher than their critical micelle concentration (CMC).

2.2 Microfluidic device fabrication

Two identical T-junction microchannels, one for each kind of surfactant solution, were both fabricated on 60 mm ×

Table 1 Physical properties of working systems in the experiment at 25 °C

Solution	Viscosity μ_w (mPa s)	Contact angle θ (°)	Static interfacial tension γ_{eq} (mN/m)
0.5 wt% SDS	0.90	19.8	5.0
1.0 wt% SDS	0.93	14.4	
2.0 wt% SDS	0.99	10.0	
4.0 wt% SDS	1.11	6.1	
6 wt% Tween 20	1.87	25.0	5.3
12 wt% Tween 20	2.42	19.2	
18 wt% Tween 20	4.26	10.0	

30 mm × 4 mm poly(methyl methacrylate) (PMMA) chips using a CNC drill device. They were designed to adapt to the pressure measurement platform, with two ports connected to the pressure drop sensor as shown in Fig. 1. The dimensions of all the microchannels were 620 μm width × 600 μm depth. Another 60 mm × 30 mm × 4 mm PMMA chip was sealed over the microchannels at 75 °C 0.4 MPa, using a thermal sealing machine (A274, Techson, China). Prior to any experiments, the microchannels were filled with the continuous phases for at least 4 h to avoid the wetting effect of the dispersed phase.

2.3 Online pressure drop measurement platform

The online pressure drop measurement platform is composed by commercial pressure drop sensor (DP86-001D, USA), electronic circuit amplifier (self-made), and oscilloscope (DOS3064, Hantek, China) connected to PC as shown in Fig. 2. A vibration isolation shelf is also designed to reduce the ambient mechanical signal noise. In our previous studies, we found this pressure drop measurement platform worked well with error less than a few Pascal for droplet generation frequency below 25 Hz (Riaud et al. 2013). With this apparatus, we can observe both the

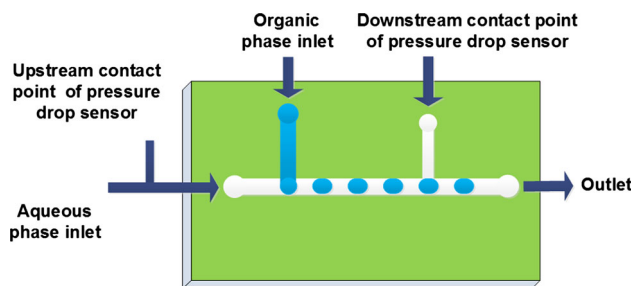


Fig. 1 The structure of microchannel device. The first T-junction microchannel is used to form microdroplets. The second one and the bifurcate feeding pipe are used to connect the pressure drop sensor

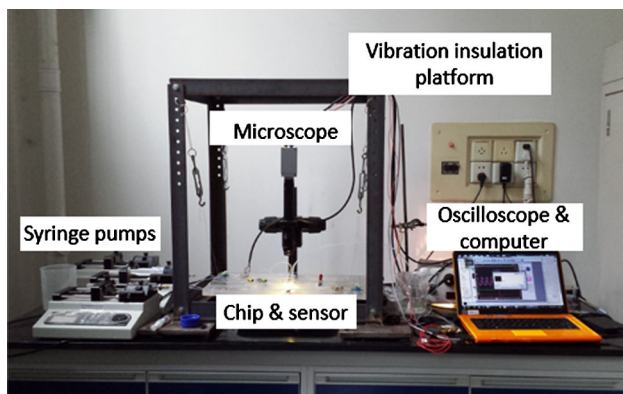


Fig. 2 The pressure drop measurement platform in laboratory

constant pressure drop of Poiseuille flow in a rectangular microchannel and the pressure drop fluctuation during the bubble generation in a T-junction microchannel. A microscope with a 10× objective lens and an attached CMOS camera (PixeLINK 742U, Canada) was used to observe flows in real time at the T-junction. Videos were recorded at a speed of 270 fps in the experiment. A self-made synchronizer was used to collect the video and the pressure drop waveform at the same time. Experiments were conducted using two separated syringe pumps (LSP02-1B, Longer, China) to control the liquids' flow rates. Different flow rates of the dispersed phase (12.5–350 μL/min) and continuous phase (50–1,400 μL/min) were effectuated with a constant flow rate ratio of 1:4.

3 Results and discussion

3.1 Flow region and droplet size variation

Previous studies have shown that in a T-junction, the breakup of plug-shaped droplet is mainly dominated by pressure accumulation as it is generated (Garstecki et al. 2006). It is also indicated that in case of small capillary number ($Ca < 0.01$) or squeezing regime, the droplet volume is in a linear relation with the flow rate ratio of the dispersed phase to the continuous phase Q_O/Q_W , $L/w = a \cdot Q_O/Q_W + b$. However, according to our experimental results, at constant flow rate ratio ($Q_O/Q_W = 1/4$), the droplet length still changed with the vicious shearing effect of continuous phase even in the case of very small evaluated capillary number ($Ca = 0.0004–0.04$, based on the static interfacial tensions of working systems). The explanation could be that Q_O/Q_W is much smaller than 1 in our case, which is not the case in the work of Garstecki et al. (2006). Therefore, the operating region in our study is in the transition region between squeezing flow and dripping flow which has been reported in many previous papers (Christopher et al. 2008; Xu et al. 2008; Glawdel et al. 2012a). In this flow region, the dimensionless droplet length L/w is a function of both two-phase flow ratio and capillary number of continuous phase. As the phase ratio is constant at 1/4 in the present experiment, the only variable is the capillary number of the continuous phase.

As we doubted that there was dynamic interfacial tension issue during the droplet generation process, the droplet length and the characterized shearing force of continuous phase ($\mu_w Q_w / wh$) were firstly plotted to show the effect of surfactant concentrations in Fig. 3a, b. It is obvious that shear force plays an important role in determining droplet length in our experiments. Also, we can clearly see that there is nearly no difference of droplet lengths in different continuous phases composition at a constant shearing

force, except the 6 wt% Tween 20 experiment at $\mu_w Q_w / wh < 0.04$, which means the interfacial tensions at the droplet breakup moment are almost the same for different working systems. Using the static interfacial tensions to calculate the capillary number as many previous works did, we regress the non-dimensional droplet lengths versus Ca as a power law:

$$L/w = 0.58Ca^{-0.25}. \quad (2)$$

The calculated curve from Eq. 2 is shown in Fig. 3c, exhibiting the power law fits well with experimental data.

3.2 Pressure drop fluctuation during droplet generation

According to the droplet length at the end of droplet generation process, the interfacial tension is seemed equal to the static interfacial tension for all the working systems. However, in the early stage of droplet growth at the T-junction, we find different dynamic interfacial tensions still exist. Using the pressure measurement platform, we can observe this phenomenon. According to the experimental results, two parts contribute to the total pressure drop ($P = P_s + \Delta P$): One is the steady pressure drop (P_s) caused by the two-phase flow resistance in microchannel, and the other is the fluctuating pressure drop (ΔP) caused by interface evolution during the droplet generation. As shown in the Appendix 1, flow droplets were shown to have no detectable effect on the

pressure drop measurement. In a droplet generation period, we observed the total pressure drop first increased quickly. After reaching a maximum value, the total pressure drop decreased and reached P_s with the breakup of two-phase interface. As shown in Fig. 4a, the measured pressure drop has noises and we used a mathematical smoothing method to show the variation of the pressure drop. The difference between the total pressure drop and the steady pressure drop defines the fluctuating pressure drop (ΔP) caused by the Laplace pressure of two-phase interface, which can be represented by Eq. 1 (Riaud et al. 2013). Figure 4a shows the evolution of pressure drop when continuously forming octane droplets in 6 wt% Tween 20 aqueous solution. In this figure, the pressure drop is periodic, corresponding to the droplet generation frequency. Figure 4b shows the pressure drop in one droplet generation period and its relation with the droplet growing stage. From point A to point B(C), the pressure drop increases with the filling of the main channel by the dispersed phase. From point B(C) to point E, the pressure drop decreases due to the stretching and breakup of the interface. We found the highest pressure drop is almost taking place at the end of filling stage defined by Glawdel et al. (2012a), where the interface starts to leave the wall of T-junction side channel.

Figure 5a, b show the average values and experimental errors of all the maximum fluctuated pressure drops (ΔP_{\max}) at different operating conditions in at least 10

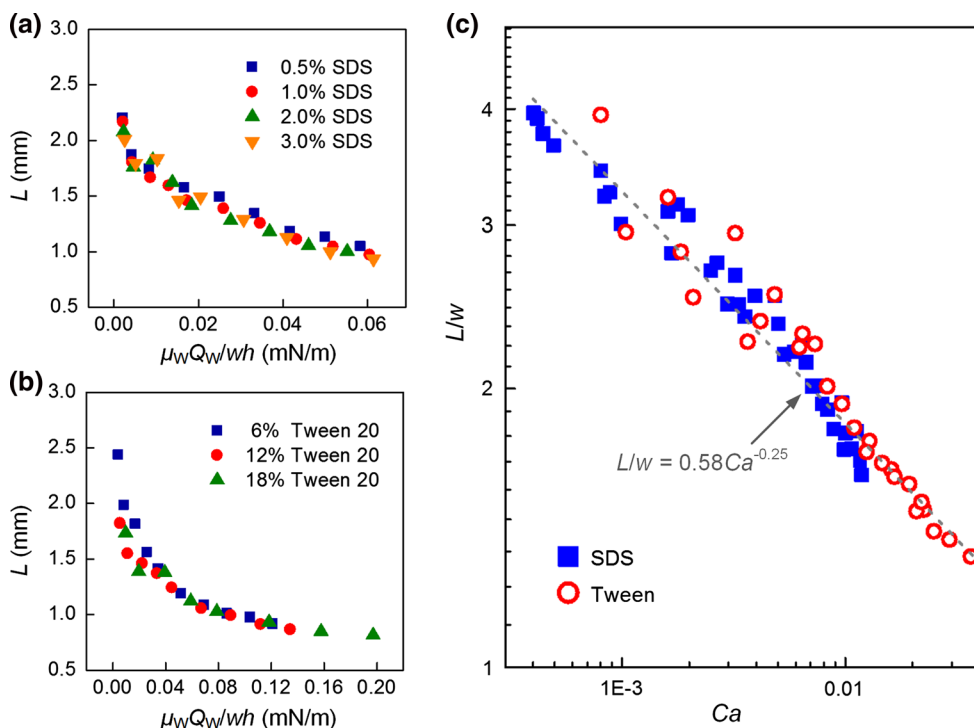


Fig. 3 Length variation of droplets at different operating conditions. **a, b** Droplet lengths with the variation of characterized shearing force. **c** Comparisons of non-dimensional droplet lengths with the variation of Ca for all experiments. The dashed line is Eq. 2

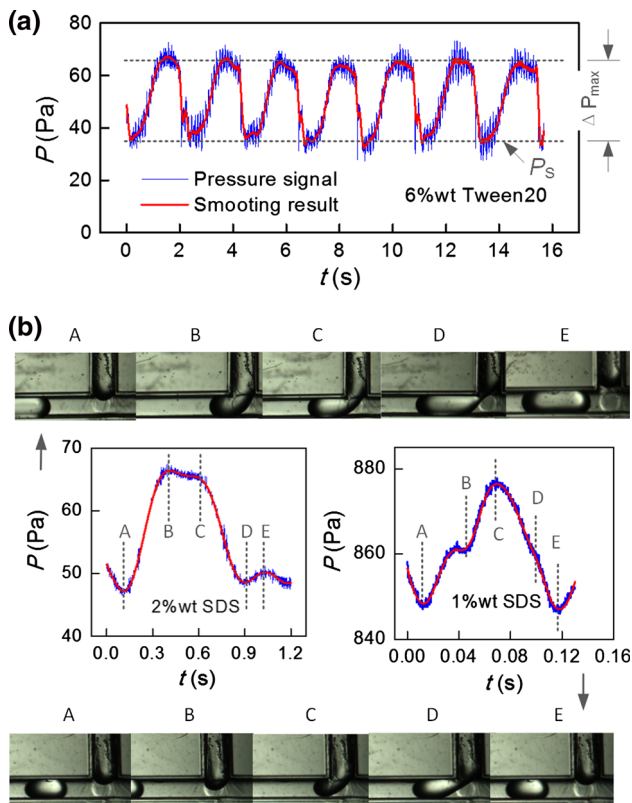


Fig. 4 Pressure drop measurement results and their synchronous microscope pictures. **a** Pressure drop waveform of continuously forming droplets. The amplitude of the smoothing data (Savitzky–Golay method with 100 dots as samples using two-order polynomial smoothing equations) shows the maximum pressure drop. The working system is octane/6 wt% Tween 20 solution system at $Q_O = 12.5 \mu\text{L}/\text{min}$, $Q_W = 50 \mu\text{L}/\text{min}$. **b** The microscope pictures and pressure drop fluctuations in a fluctuation period. Points A–E reflect different droplet growing stages. The working system is octane/2 wt% SDS solution systems at $Q_O = 12.5 \mu\text{L}/\text{min}$, $Q_W = 50 \mu\text{L}/\text{min}$ (top-left) and octane/1 wt% SDS solution systems at $Q_O = 200 \mu\text{L}/\text{min}$, $Q_W = 800 \mu\text{L}/\text{min}$ (bottom-right)

droplet formation periods. Interestingly, all the pressure drop dots have tortuous raising tendencies with the increase of two-phase flow rate: The general trend is that ΔP_{max} firstly increases and then reaches a little falling between 500 and 1,000 $\mu\text{L}/\text{min}$. Finally, the maximum pressure drop begins to increase again at higher flow rate. This is very different from the constant interfacial tension system as shown in Appendix 2. To figure out this special experimental phenomenon, we checked our recorded videos and found two growing droplet states in the experiment as shown in Fig. 4b. One state exhibits the growing droplet blocking the channel section before the highest pressure drop point, and the other state shows a unblock channel section with a bypass flow of continuous phase at the bottom of the channel. These two droplet states have different interface curvature radii, and the transition point of them is between 500 and 1,000 $\mu\text{L}/\text{min}$.

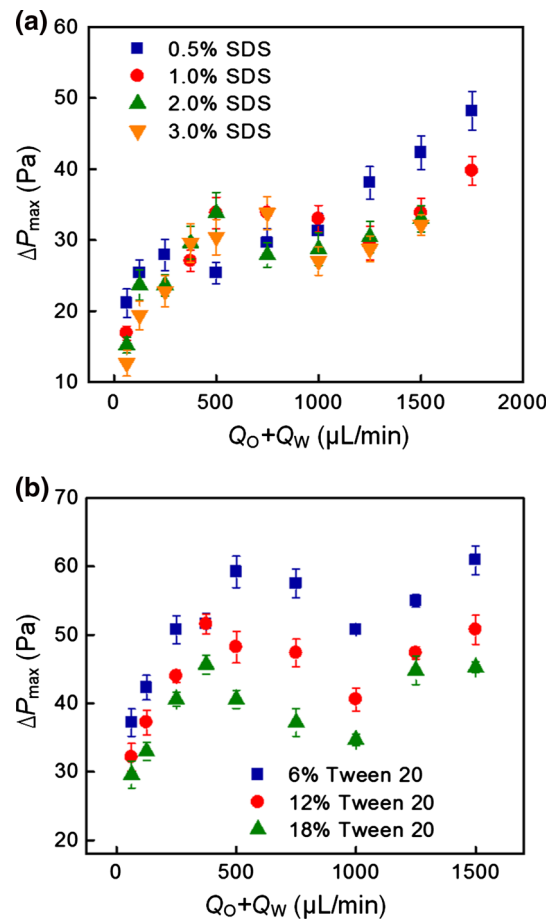


Fig. 5 Maximum pressure drops at different operating conditions. The variation of average maximum pressure drop with the changing of two-phase flow rate. The pressure drops are average values in at least 10 droplet generation processes. Error bars signify the range between the largest and the smallest values in 10 parallel experiments

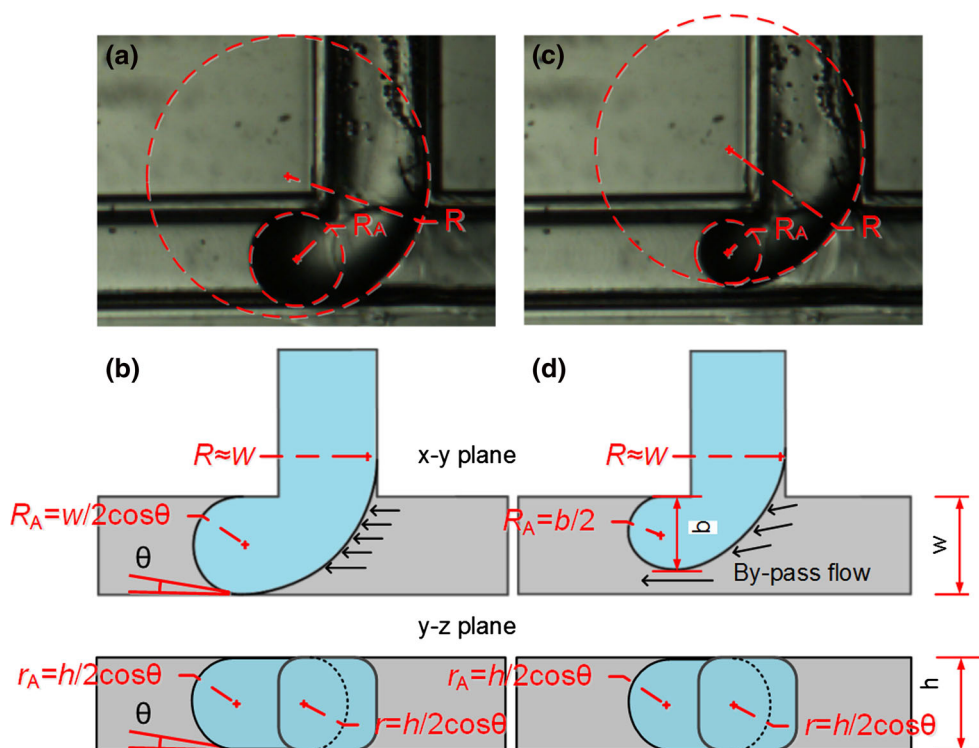
3.3 Determination of dynamic interfacial tension

According to our observations on the droplet generation period, the pressure drop rises in the filling stage defined by Glawdel et al. (2012a), where the droplet starts to flow out of the side channel. During this process, the droplet starts to block the channel and the curvatures of droplet head (R_A , r_A) and droplet tail (R , r) change with time evolution. The droplet head radius (R_A) becomes smaller and smaller than the droplet tail radius (R) on x – y plane as shown in Figs. 4 and 6, causing different Laplace pressure between two sides of the droplet. At the end of the filling stage, the radii of both droplet head and tail ($r_A = r$) on the y – z plane are nearly constant at $h/(2 \cos\theta)$. Therefore, the fluctuating pressure drop at the highest pressure drop point can be simplified to

$$\Delta P = \gamma \cdot (1/R_A - 1/R). \tag{3}$$

After the filling stage of droplet generation, we observed the pressure drop decreased. According to the work of van

Fig. 6 Pictures and sketch diagrams of the highest pressure drop moment with and without blocking channel by growing droplets. **a, b** An experimental picture and its sketch diagrams of the droplet blocking the channel section. **c, d** An experimental picture and its sketch diagrams of the droplet with bypass continuous phase flow



Steijn et al. (2010) and our previous analysis (Riaud et al. 2013), the droplet head radius on the y - z plane and the radii of both droplet head and tail on the x - y plane will not change very much, but the droplet tail radius on the y - z plane decreases quickly with the stretching of interface. In this situation, the fluctuated pressure drop changes to

$$\Delta P \approx \gamma \cdot (1/R_A + 2 \cos \theta/h - 1/R - 1/r). \quad (4)$$

With keeping the decreasing of r in Eq. 4, ΔP decreases quickly and becomes to zero at the breakup moment.

Theoretically, the interfacial tension at any moment during a droplet generation process can be calculated with accurate pressure drop experiment and the above two equations. However, we cannot directly obtain $1/r$ in Eq. 4 from common 2D observation, which currently restricts the application of this method. Using the pressure measurement method, we limit our analysis to the filling stage using Eq. 3 in this paper with the ΔP_{\max} we provided above. According to the geometries of droplet blocking and unblocking the channel section at the highest pressure drop moment, Eq. 3 can be decomposed to Eqs. 5 and 6

$$\Delta P_{\max} \approx \gamma \cdot (2/w \cos \theta - 1/R) \quad \text{blocking channel} \quad (5)$$

$$\Delta P_{\max} \approx \gamma \cdot (2/b - 1/R) \quad \text{by-pass flow} \quad (6)$$

where b is the filling depth of the droplet as shown in Fig. 6d. Equations 5 and 6 are good tools to evaluate the pressure drop in droplet generation process. However, in order to make sure of the interfacial tension accuracy, we

directly used the measured radii of R_A and R from recorded pictures in calculation, as shown in Fig. 6a, b, and the results are given in Fig. 7. According to the droplet length analysis in Sect. 3.1 at droplet breakup point, the interfaces are seemed saturated, at the ΔP_{\max} point; however, the adsorption is far from complete for both SDS and Tween 20. Putting aside the first experimental point for 4 %wt SDS solution, other points all have an instantaneous interfacial tension larger than the static value ($\gamma_{\text{eq}}^{\text{SDS}} = 5.0 \text{ mN/m}$, $\gamma_{\text{eq}}^{\text{Tween20}} = 5.3 \text{ mN/m}$), due to the un-finished adsorption of surfactant in the initial droplet formation stage.

3.4 Adsorption of surfactant

In Fig. 7, the interfacial tension generally increases with the total flow at moderated value, but decreases at larger flow rate, except for the lowest 0.5 wt% concentration of SDS solution. The transition point is near 500 $\mu\text{L}/\text{min}$, fixed by the droplet growth state transition point we discussed above. According to the study of Glawdel et al. (2012b), the mass transfer of surfactant in dispersed phase during droplet generation in squeezing–dripping transitional flow is mainly controlled by the diffusion rate of surfactant. However, in our previous studies, we found that the convection of two phases cannot be omitted especially for working system contained surfactant in the continuous phase (Wang et al. 2009). In order to determine the main influencing factors on the dynamic interfacial tension, we

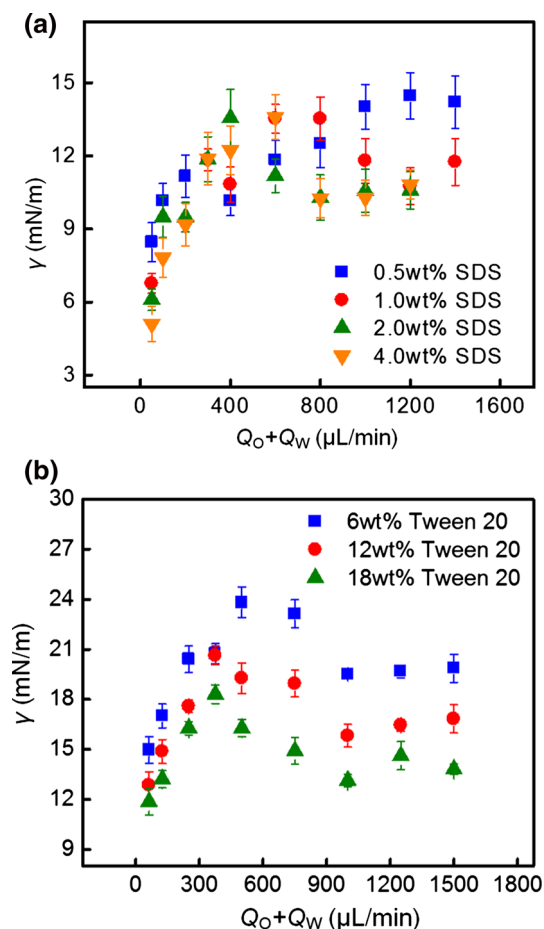


Fig. 7 Dynamic interfacial tensions at different operating conditions. The calculated instantaneous interfacial tensions at the highest pressure drop moment with the changing of two-phase flow rate. The interfacial tensions are average values of at least 10 droplet generation processes. *Error bars* signify the range between the largest and the smallest values

plot the interfacial tension difference $\gamma - \gamma_{eq}$ versus $(\pi D/4t)^{1/2}$, which signifies the mass transfer coefficient according to the penetration theory of Higbie (1935). Figure 8 gives the results. In this figure, we can see the interfacial tension first increases with $(\pi D/4t)^{1/2}$, but then slightly decreases. According to the experimental pictures, this transition point corresponds to the critical point that the droplet blocking channel at the highest pressure drop moment. This phenomenon implies different mechanisms of surfactant adsorption.

For a surfactant whose concentration is above the CMC, the adsorption proceeds in three steps: the micelle dissolution, the diffusive or convective mass transfer of surfactant, and the interface adsorption equilibrium (Alvarez et al. 2010; Brosseau et al. 2014). For the SDS solution system, at $(\pi D/4t)^{1/2} < 10^{-4}$ m/s, our data seemed corresponding with the diffusion-controlled adoption equation given by Eastoe and Dalton (2000),

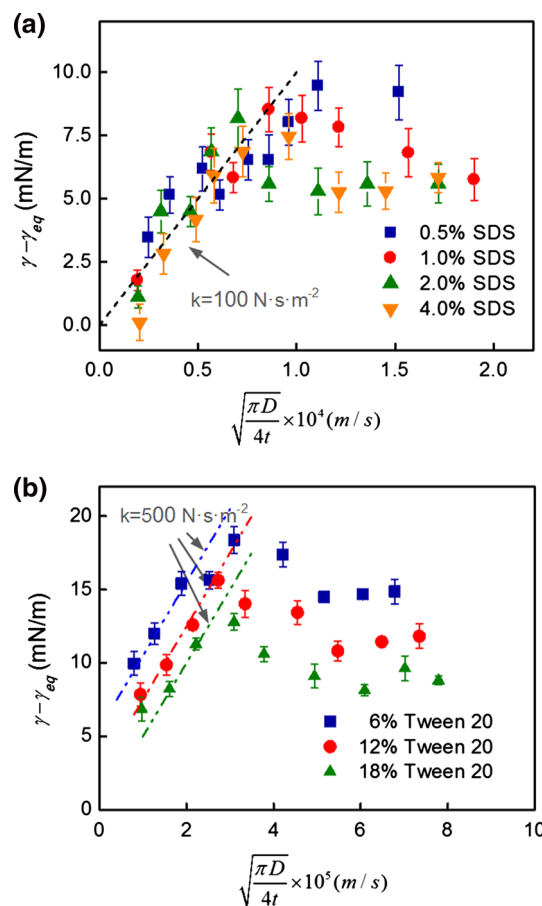


Fig. 8 Dimensionless interfacial tension with the variation of droplet growth time. The droplet growth time t represents the time between last interface breakup to the highest pressure drop point in the experiment. The *dash line* in **a** has a slop of 100 Ns/m², and all the *dash line* in **b** has a slop of 500 Ns/m². The diffusion coefficients are 9.6×10^{-10} m²/s for SDS according to Glawdel and Ren (2012) and 9.3×10^{-11} m²/s for Tween 20 according to Carnero Ruiz et al. (2003)

$$\gamma - \gamma_{eq} \sim \frac{RT\Gamma_{eq}^2}{CD} \sqrt{\frac{D\pi}{4t}} = k\sqrt{\frac{D\pi}{4t}} \tag{7}$$

where Γ_{eq} is the saturated adsorbing capacity of surfactant on the interface, C is the surfactant monomer concentration, and D is the diffusion coefficient of surfactant. From Fig. 8, we can clearly see that there is a linear relation between $\gamma - \gamma_{eq}$ and $(\pi D/4t)^{1/2}$ at $(\pi D/4t)^{1/2} < 10^{-4}$ m/s. The concentration of SDS has little effect on the dynamic interfacial tension, reflecting the surfactant monomer concentration is stable in these solutions; thus, the SDS micelle dissolution is fast. The dashed line in Fig. 8a is a correlated formula:

$$\gamma - \gamma_{eq} = k\sqrt{\frac{D\pi}{4t}}, \quad k = 100 \text{ (Ns/m}^2\text{)} \tag{8}$$

Equation 8 is seemed obey the basic diffusion-controlled model given by Eq. 7. But during the calculation

process, we found the slope k is much larger than the theoretical value of $RT\Gamma_{\text{eq}}^2/CD$, which is 2.4 N s/m^3 for the SDS system ($\Gamma_{\text{eq}} = 3 \times 10^{-6} \text{ mol/m}^2$). We guess the reason is the different growth process of droplet in flowing continuous phase comparing to the static droplet in the interfacial tension meter. The interface movement causes non-uniform distribution of surfactant on droplet surface (Baret et al. 2009), which makes the whole process much more complex, and we therefore do not obtain a pure diffusion-controlled equation. For a more precisely express, we called surfactant adsorption rule in the blocking channel filling stage “quasi-diffusion-controlled process” in this paper. For the Tween 20 system, in spite of the three solutions exhibiting linear relation between $\gamma - \gamma_{\text{eq}}$ and $(\pi D/4t)^{1/2}$, it should be noticed that they do not have a tendency passing through the origin point and obviously, the Tween 20 concentration has strong influence on the interfacial tension even when the concentration exceeds a thousand times the CMC. Hence, we believe the adsorption is limited by the low micelle dissolution rate. Three evaluated lines are provided in Fig. 8b with the following equation just to show the interfacial tension variation tendency at $(\pi D/4t)^{1/2} < 3 \times 10^{-5} \text{ m/s}$

$$\begin{aligned} \gamma - \gamma_{\text{eq}} &= k\sqrt{\frac{D\pi}{4t}} + b, \quad k = 500 \text{ (N s/m}^2\text{)}, \\ b &= 5.5, 2.5, 0 \times 10^{-3} \text{ (N/m)} \end{aligned} \quad (9)$$

When the growing droplet cannot block the main channel at the filling stage, the quasi-diffusion limited curve does not fit our data anymore. The calculated interfacial tension decreases with the increase of the two-phase flow rate, which implies that convection dominates the mass transfer of surfactant. This convection should happen at the open corner of the channel, and it is enhanced at high flow rates by the reduction of the filling depth of the growing droplet (b). Comparing the two surfactants SDS and Tween 20, it is clear that the adsorption of small ionic surfactant is faster than the big neutral ones. In microfluidic droplet generation studies using the SDS aqueous solution, several times higher concentration than its CMC is enough; however, the concentration of Tween 20 should be much higher than its CMC due to its poor mass transfer performance and low micelle dissolution rates.

4 Conclusion

In this paper, we introduce a pressure drop measurement method assisted by simple image analysis to determinate the dynamic interfacial tension during the droplet generation process in a T-junction microchannel. Using the relation between Laplace pressure and the fluctuation pressure drop,

we calculate the instantaneous interfacial tension at the highest pressure drop point and find this apogee coincides with the end of the filling stage of droplet growth defined by Glawdel et al. (2012a) as the liquid–liquid interface starts to leave the side channel. By analyzing the dynamic interfacial tension, we find that although the surfactant nearly finished its adsorption process at the rupturing moment, there is still dynamic interfacial tension phenomenon in the initial droplet filling stage of liquid–liquid squeezing–dripping transition flow. This result shows the advantage of the pressure measurement method compared with our previous droplet size method (Wang et al. 2009). The variation of interfacial tension exhibits quasi-diffusion-controlled rules at the situation that the growing droplet blocks entirely the channel section prior to reaching the highest pressure drop. However, once the blockage cannot be totally achieved due to high flow rate, this model no longer works. The strong convection flow caused reduction of interfacial tension. Surfactant SDS and Tween 20 also show some discrepancy in the mass transfer rate and micelle dissolution rate. The SDS concentration has little effect on the dynamic interfacial tension, but low concentrations of Tween 20 causes high value. Nonetheless, surfactant adsorption is a complicated process, and we will enforce ourselves to develop new method to reveal the 3D interface evolution during the droplet generation, which is helpful for improving the pressure measurement method.

Acknowledgments We would like to acknowledge the support of the National Natural Science Foundation of China (21036002, 91334201, U130227) for this work.

Appendix 1

To eliminate the possibility that pressure drop fluctuation comes from passing droplet over the sensor, we designed another microchannel that was identical as the one in Fig. 1, except the position of pressure measurement points: Instead of measuring the upstream and downstream of a T-junction, here we focused on the two-phase flow in the straight microchannel. Two pressure measurement points were placed at the downstream of the T-junction with a distance of 20 mm. In annex test, Q_C and Q_D were chosen at 200 and 50 $\mu\text{L/m}$ to make sure that there is only one droplet at each between A and B, as shown in Fig. 9.

First of all, the blank experiment was conducted without the feeding of dispersed phase. About 2 % SDS–water solution was pumped into the microchannel at 200 $\mu\text{L/m}$, and the pressure drop was shown by bottom line in Fig. 9. Small fluctuation whose amplitude $< 1 \text{ Pa}$ came from the mechanic and electronic noises, which have been commonly observed in our experiment. Then, the two-phase

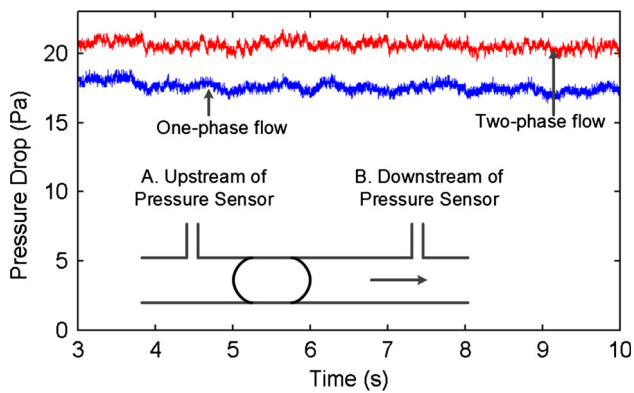


Fig. 9 Pressure drop of droplet flow passing over the pressure drop sensor

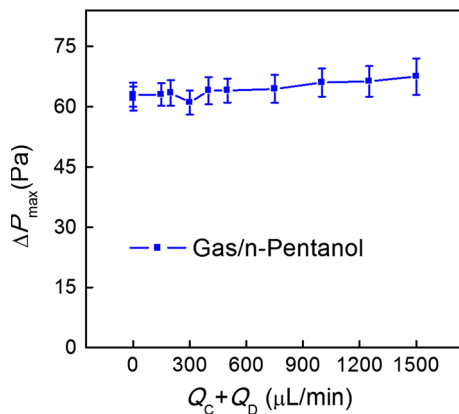


Fig. 10 ΔP_{\max} in gas/n-pentanol system without surfactant

flow was carried out at $Q_C = 200 \mu\text{L}/\text{m}$ and $Q_D = 50 \mu\text{L}/\text{m}$. Droplet was generated at 0.67 Hz. The corresponding pressure drop we measured is given by the top line in Fig. 9. No evident periodic pressure fluctuation (ΔP) like Fig. 4 was observed in the two-phase flow, and the only difference was just the constant steady pressure drop (P_S). This is just because of the increase of total flow rate. According to this experiment, we can conclude that droplet that passes over the sensor would not have an obvious influence on the pressure drop measurement during droplet generation.

Appendix 2

To verify the “pressure drop-based method,” we used air/n-pentanol system to do a calibration experiment, which did not have surfactant. All the operating conditions are nearly the same as above statement, such as the flow ratio and channel treating time (for the wetting property). From Fig. 10, we can see that ΔP_{\max} is almost unchanged comparing to Fig. 5, due to the unchanged interfacial tension.

Using Eqs. 3 and 4, we obtain the surface tension of n-pentanol: 25.8 mN/m, which is close to the reported value 24.75 mN/m in the book from Riddick (1986).

References

- Abate RA, Mary P, van Steijn V, Weitz DA (2012) Experimental validation of plugging during drop formation in a T-junction. *Lap Chip* 12:1516–1521. doi:10.1039/c2lc21263c
- Alvarez NJ, Walker LM, Anna SL (2010) A microtensiometer to probe the effect of radius of curvature on surfactant transport to a spherical interface. *Langmuir* 26(16):13310–13319. doi:10.1021/la101870m
- Baret JC (2012) Surfactants in droplet-based microfluidics. *Lab Chip* 12(3):422–433. doi:10.1039/C1LC20582J
- Baret JC, Kleinschmidt F, El Harrak A, Griffiths AD (2009) Kinetic aspects of emulsion stabilization by surfactants: a microfluidic analysis. *Langmuir* 25(11):6088–6093. doi:10.1021/la9000472
- Beebe DJ, Mensing GA, Walker GM (2002) Physics and applications of microfluidics in biology. *Annu Rev Biomed Eng* 4:261–286. doi:10.1146/annurev.bioeng.4.112601.125916
- Brosseau Q, Vignon J, Baret JC (2014) Microfluidic dynamic interfacial tensiometry (μDIT). *Soft Matter* 10(17):3066–3076. doi:10.1039/c3sm52543k
- Carnero Ruiz C, Molina-Bolivar JA, Aguiar J, MacIsaac G, Moroz S, Palepu R (2003) Effect of ethylene glycol on the thermodynamic and micellar properties of Tween 20. *Colloid Polym Sci* 281:531–541. doi:10.1007/s00396-002-0801-1
- Christopher GF, Anna SL (2007) Microfluidic methods for generating continuous droplet streams. *J Phys D Appl Phys* 40:R319–R336. doi:10.1088/0022-3727/40/19/R01
- Christopher GF, Noharuddin NN, Taylor AJ, Anna LS (2008) Experimental observations of the squeezing-to-dripping transition in T-shaped microfluidic junctions. *Phys Rev E* 78:036317. doi:10.1103/PhysRevE.78.036317
- Cristini V, Tan YC (2004) Theory and numerical simulation of droplet dynamics in complex flows—a review. *Lab Chip* 4:257–264. doi:10.1039/B403226H
- Dong PF, Xu JH, Zhao H, Luo GS (2013) Preparation of 10 μm scale monodispersed particles by jetting flow in coaxial microfluidic devices. *Chem Eng J* 14:106–111. doi:10.1021/ja042494w
- Eastoe J, Dalton JS (2000) Dynamic surface tension and adsorption mechanisms of surfactants at the air–water interface. *Adv Colloid Interface* 85(2):103–144. doi:10.1016/S0001-8686(99)00017-2
- Garstecki P, Fuerstman MJ, Stone HA, Whitesides GM (2006) Formation of droplets and bubbles in a microfluidic T-junction—scaling and mechanism of break-up. *Lab Chip* 6:437–446. doi:10.1039/B510841A
- Glawdel T, Ren CL (2012) Droplet formation in microfluidic T-junction generators operating in the transitional regime. III. Dynamic surfactant effects. *Phys Rev E* 86(2):026308. doi:10.1103/PhysRevE.86.026308
- Glawdel T, Elbuken C, Ren CL (2012a) Droplet formation in microfluidic T-junction generators operating in the transitional regime. I. Experimental observations. *Phys Rev E* 85(1):016322. doi:10.1103/PhysRevE.85.016322
- Glawdel T, Elbuken C, Ren CL (2012b) Droplet formation in microfluidic T-junction generators operating in the transitional regime. II. Modeling. *Phys Rev E* 85(1):016323. doi:10.1103/PhysRevE.85.016323
- Higbie R (1935) The rate of absorption of a pure gas into a still liquid during short periods of exposure. *Trans Am Inst Chem Eng* 35:36–60

- Kobayashi I, Nakajima M, Chun K, Kikuchi Y, Fujita H (2001) Silicon array of elongated through-holes for monodisperse emulsion droplets. *AIChE J* 48:1639–1644. doi:[10.1002/aic.690480807](https://doi.org/10.1002/aic.690480807)
- Mikati N (1993) Diffusion of sodium dodecyl sulfate studied by a steady-state technique. *Langmuir* 9:113–116. doi:[10.1021/la00025a026](https://doi.org/10.1021/la00025a026)
- Riaud A, Tostado PC, Wang K, Luo GS (2013) A facile pressure drop measurement system and its applications to gas–liquid microflows. *Microfluid Nanofluid* 15(5):715–724. doi:[10.1007/s10404-013-1174-0](https://doi.org/10.1007/s10404-013-1174-0)
- Riddick JA (1986) *Organic solvents: physical properties and methods of purification*. Wiley, New York
- Thorsen T, Roberts R, Arnold F, Quake S (2001) Dynamic pattern formation in a vesicle-generating microfluidic device. *Phys Rev Lett* 86:4163–4166. doi:[10.1103/PhysRevLett.86.4163](https://doi.org/10.1103/PhysRevLett.86.4163)
- Thorsen T, Maerkl SJ, Quake SR (2002) Microfluidic large-scale integration. *Science* 298:580–584. doi:[10.1126/science.1076996](https://doi.org/10.1126/science.1076996)
- van der Graaf S, Schroen CGPH, van der Sman RGM, Boom RM (2004) Influence of dynamic interfacial tension on droplet formation during membrane emulsification. *J Colloid Interface Sci* 277(2):456–463. doi:[10.1016/j.jcis.2004.04.033](https://doi.org/10.1016/j.jcis.2004.04.033)
- van Steijn V, Kleijn CR, Kreutzer MT (2010) Predictive model for the size of bubbles and droplets created in microfluidic T-junctions. *Lab Chip* 10:2513–2518. doi:[10.1039/C002625E](https://doi.org/10.1039/C002625E)
- Wainright A, Nguyen UT, Bjornson T, Boone TD (2003) Preconcentration and separation of double-stranded DNA fragments by electrophoresis in plastic microfluidic devices. *Electrophoresis* 24:3784–3792. doi:[10.1002/elps.200305594](https://doi.org/10.1002/elps.200305594)
- Wang K, Lu YC, Xu JH, Luo GS (2009) Determination of dynamic interfacial tension and its effect on droplet formation in the T-junction microdispersion process. *Langmuir* 25:2153–2158. doi:[10.1021/la803049s](https://doi.org/10.1021/la803049s)
- Whitesides GM (2006) The origins and the future of microfluidics. *Nature* 442(7101):368–373. doi:[10.1038/nature05058](https://doi.org/10.1038/nature05058)
- Xu Q, Nakajima M (2004) The generation of highly monodisperse droplets through the breakup of hydrodynamically focused microthread in a microfluidic device. *Appl Phys Lett* 85:3726–3728. doi:[10.1063/1.1812380](https://doi.org/10.1063/1.1812380)
- Xu JH, Li SW, Tan J, Wang YJ, Luo GS (2008) Correlations of droplet formation in T-junction microfluidic devices: from squeezing to dripping. *Microfluid Nanofluid* 5:711–717. doi:[10.1007/s10404-008-0306-4](https://doi.org/10.1007/s10404-008-0306-4)
- Xu K, Tostado CP, Xu J, Lu Y, Luo G (2014) Direct measurement of the differential pressure during drop formation in a co-flow microfluidic device. *Lab Chip* 14(7):1357–1366. doi:[10.1039/c3lc51222c](https://doi.org/10.1039/c3lc51222c)